Supporting information

Improving the Ecological Index in the Solution Processing of Hybrid Perovskites

Niusha Heshmati, Niklas Almandinger, Thomas Fischer and Sanjay Mathur*.

Institute of Inorganic and materials Chemistry, Department of Chemistry, University of Cologne, Cologne, Germany.

**Corresponding author. Email: sanjay.mathur@uni-koeln.de*

1 Experimental Details

1.1 Perovskite solution preparation

The perovskite precursor solutions were produced under inert atmosphere in an *Mbraun Labmaster 130* glovebox with *MB20G* gas purifying system. For preparation of 0.8 M reference $Cs_{0.05}(MA_{0.17}FA_{0.83})_{0.95}Pb(I_{0.83}Br_{0.17})_3$ perovskite precursors were dissolved in DMF:DMSO 80:20 vol% solvent mixture.[1] The solution was heated at 50°C for 30 minutes and were filtered using a 0.22 µm PTFE filter.

The optimized green solvent solutions were prepared with same 0.8 M concentration and addition of 20 wt% MACl salt in Cy-THF:DMSO 70:30 vol%. For the solvent blending acetonitrile as an additive was added from 0 to 12.5 vol% to the solvent mixture, and 7.5 vol% was chosen as an optimum percentage. The perovskite salts were fully dissolved by heating at 50°C for 30 minutes. Once a clear solution was obtained, 20 wt% thiourea was added as a dopant, followed by stirring for an additional 30 minutes. Finally, the resulting clear-yellow solutions were filtered using a 0.22 µm PTFE filter.

1.2 Methods

X-ray diffractometry (XRD) was conducted using a *Stoe X-ray diffractometer* with *Cu Kα1* radiation (λ = 1.54062 Å). Data analysis was carried out with the WinXpow software (version 1.10) from STOE & Cie GmbH.

UV/Vis spectroscopy was performed to measure the absorption of the fabricated perovskite films using a *Cary 60 UV/Vis spectrophotometer (Agilent) and a Lambda 950 UV/Vis spectrophotometer (PerkinElmer)*.

Photoluminescence (PL) spectroscopy was conducted using an *Edinburgh Instruments FLSP920 fluorescence spectrometer* equipped with a xenon arc discharge lamp and double monochromators for both excitation and emission. The excitation wavelength ranged from 465 to 470 nm. The emission detector was positioned at a 90° angle horizontally relative to the light source, with both set at a 45° horizontal angle to the sample holder. Additionally, the sample in the holder was tilted 45° in the vertical direction, resulting in excitation and detection at a 60° angle relative to the sample surface.

Scanning electron microscopy (SEM) was performed using two different instruments to analyze the film surface quality: a *Nova NanoSEM (FEI)* and a *ZEISS Sigma 300 VP*.

Dynamic light scattering (DLS) measurements were performed using a *Zetasizer Ultra Red (Malvern Panalytical)*. Each measurement was conducted with 3 mL of the precursor solution.

Contact angle measurements were conducted using a *Drop Shape Analyzer DSA 100 (Krüss)*.

Atomic force microscopy (AFM) was used to analyze the surface topography of the thin films using an *NX10 microscope (Park Systems)*.

Nuclear magnetic resonance (NMR) spectroscopy (^{1}H: 300 MHz)) was performed using a *Bruker AV 300 spectrometer*. Spectra were recorded at room temperature, and chemical shifts were reported in parts per million (ppm) relative to tetramethylsilane (TMS), with referencing to residual protons of the NMR solvent (DMSO, δ 2.50).

Fourier-Transform Infrared Spectroscopy (FTIR) measurements were recorded on a *PerkinElmer 400 FTIR* spectrophotometer.

Solar cell characterization and photocurrent-voltage (I-V) measurements were performed at ambient temperature and under air conditions using a *Keithley 2400 SourceMeter*. A 100 W LED

lamp with a color temperature of 5800 K (1 sun, calibrated with a silicon standard cell) was used as the light source, powered by a *Fuba electronic* power supply. Therefore, the devices were tested under simulated AM 1.5G solar illumination at 100 mW/cm² (1 sun) in both forward and reverse scans over a voltage range of 0–1.2 V with 10 mV stepwise down sweep. During measurements, metallic masks with an area of 0.15 cm² were applied to the front face of the cells. Data acquisition and analysis were conducted using *Oriel IV Test Station software.*

1.3 Device fabrication

FTO-coated glass substrates (19 × 19 mm²) were cleaned using an ultrasonic bath with a sequence of Hellmanex III: deionized water (2:98 vol%), deionized water, acetone, and isopropanol for 20 minutes each. The substrates were then dried using pressurized nitrogen gas to eliminate any remaining solvent. Finally, the substrates underwent UV-Ozone treatment for 30 minutes to ensure surface cleanliness and activation. To deposit a compact TiO_2 thin film, a solution of titanium diisopropoxide-bis(acetylacetonate) in absolute ethanol (1 : 10 vol%) was sprayed onto the preheated substrates at 450°C. The substrates were sprayed four times via nitrogen stream (pressure: 0.2 mbar) in intervals of 10 seconds and annealed for another 40 minutes at 450°C. For the mesoporous TiO_2 layer, a solution was prepared by dissolving TiO_2 nanoparticle paste (18NR-T, DYE) in absolute ethanol for a total ratio of 5:1 wt% (EtOH:TiO_2) and stirred overnight. For m-TiO_2 film deposition, 60 µL of solution were spin coated (5000 rpm, 45 sec) directly onto substrate. The substrates were dried at 100°C for 10 min prior to sintering at 500°C under ambient atmosphere for 45 minutes. For reference DMF:DMSO perovskite film deposition, 100 µL of a precursor solution was deposited onto FTO/m-TiO_2 substrates via the two-step spin coating process (1000 rpm, 10 sec following by 5000 rpm, 40 sec). After 40 seconds of spin coating, 100 µL of chlorobenzene were applied as an antisolvent. The resulting films were then annealed at 100°C for 45 minutes. For green perovskite film deposition, 100 µL of an optimized precursor solution was deposited onto FTO/m-TiO_2 substrates via the single step spin coating process (6000 rpm, 40 sec). After 35 seconds of spin coating, 200 µL of ethyl acetate were applied as antisolvent. The resulting films were then annealed from 60°C to 150°C for 20 minutes. Then, lithium doped *spiro*-OMeTAD solution was prepared with 0.072g *spiro*-OMeTAD dissolved in 1 mL of chlorobenzene and mixed with 17.5 µL of a lithium bis(trifluoromethanesulfonyl)imide (LiTFSI) solution (0.0208 g in 40 µL of acetonitrile, 1.81 M) and 28.5 µL of 4-TBP. 50 µL of HTL solution was dynamically spin-coated (4000 rpm, 30 seconds) and dried at room temperature. After drying, gold electrodes were thermally evaporated

using a *Q150TS sputtering device (Quorum Technologies)*. 90 nm gold layer was deposited through a mask defining the 0.15 cm² active solar cell area.

2 Supplementary Results and Discussion

2.1 Solvent and annealing temperature optimization

Experiments were conducted to determine the optimal percentage of Cy-THF in a Cy-THF:DMSO:DMF solvent system [(Cy-THF:X), (DMSO:20), (DMF:80-X) vol%], annealing conditions, and the appropriate antisolvent, as detailed in ***Figure S1.*** Initially, the experiments focused on $MAPbI_3$ to evaluate the optimal Cy-THF ratio that can be substituted with DMF and the corresponding annealing temperature**.** ***Figure S1.a and b*** compare Cy-THF films annealed at 130 °C and 150 °C. These temperatures were selected due to Cy-THF's higher boiling point when compared to DMF-based solvents. The films processed with green solvent-blend were compared with the reference $MAPbI_3$ solutions prepared in a DMF:DMSO mixture (80:20 vol%) and heated at 100 °C. It was found that the green solvent solutions exhibited comparable or superior absorbance compared to the reference sample for various solvent ratios at 150 °C. Notably, for films annealed at 130 °C, an increase in the percentage of Cy-THF resulted in a decrease in the absorbance spectrum compared to the reference. [2,3] Therefore, 150 °C was chosen as an annealing temperature and photoluminescence (PL) emission of these films illustrated in ***Figure S1.c***. These results demonstrate that with increasing percentage of Cy-THF, the PL is enhanced; however, it remains lower than the reference sample. There is a prominent shoulder peak at 825 nm in the PL spectra for films containing Cy-THF that can be attributed to residual phase impurities and defect states in the perovskite thin film originating from incomplete dissolution of educts.[4]

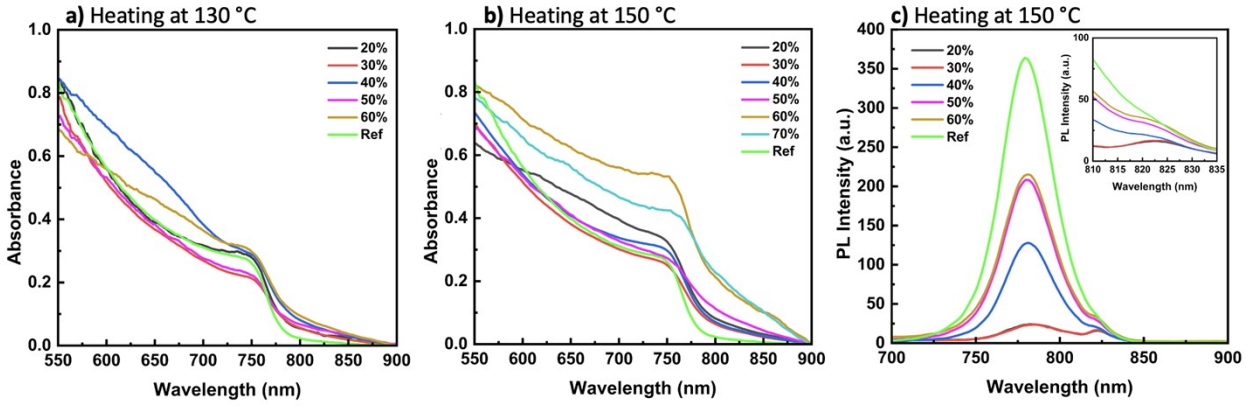

*Figure S1: Comparative analysis of $MAPbI_3$ films absorbance spectra prepared in Cy-THF:DMSO:DMF solvent system with [(Cy-THF:X), (DMSO:20), (DMF:80-X) vol%] composition and the reference sample consists of $MAPbI_3$ solution with DMF:DMSO 80:20 vol% solvent, heated at 100 °C **(a)** Upon annealing at 130 °C, UV-Vis spectra reveal slightly higher absorbance for lower percentage Cy-THF films compared to the reference film. **(b)** Upon annealing at 150 °C, all Cy-THF films exhibit higher absorbance and the more Cy-THF percentage led to the more absorbance. **(c)** Photoluminescence (PL) emission spectra of $MAPbI_3$ films showing the enhancement in PL intensity with the addition of higher 50% of Cy-THF annealed at 150 °C. All these films prepared with one step spin coating method and chlorobenzene (CB) antisolvent treatment.*

2.2 Antisolvent optimization

The antisolvent method for lead halide perovskites involves introducing a nonpolar solvent during film formation to rapidly precipitate the perovskite crystals, improving film uniformity and crystallinity by controlling the nucleation and growth process.[5] Chlorobenzene (CB), the most widely used antisolvent for LHPs was substituted due to its high toxicity. Ethyl acetate (EA), recognized as an environmentally friendly antisolvent was used and compared with CB-treated films in this work.[6] As illustrated in ***Figure S2.a***, the Cy-THF samples treated with EA antisolvent yielded similar crystallinity to CB treated film. The PL spectra, presented in ***Figure S2.b***, indicate that using EA as an antisolvent results in higher radiative recombination and a less intense double impurity peak. Therefore, EA was selected as the primary antisolvent for this study. However, the crystallinity and photoluminescence emission of the reference DMF:DMSO film treated with CB antisolvent remains higher than that of the Cy-THF ink samples.

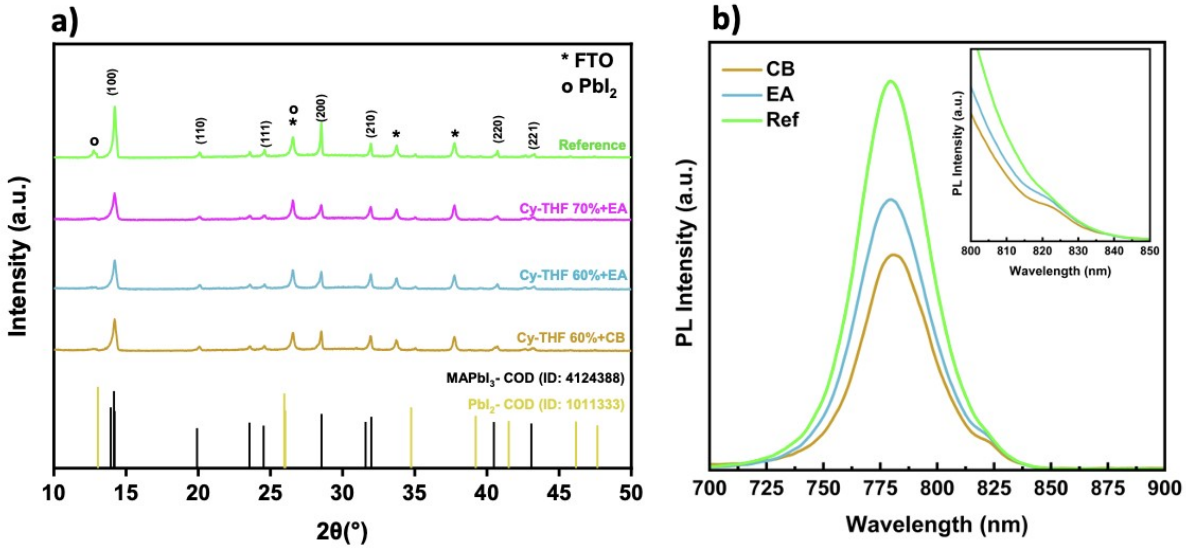

*Figure S2: **(a)** X-ray diffraction (XRD) patterns of 1M $MAPbI_3$ thin films treated with ethyl acetate (EA) and chlorobenzene (CB), compared with the DMF:DMSO reference sample. **(b)** Photoluminescence (PL) spectra of Cy-THF:DMSO:DMF 70:20:10% film at room temperature treated with EA and CB at room temperature compared with reference sample. The higher PL emission in the EA-treated film suggests improved charge recombination efficiency.*

2.3 Nuclear Magnetic Resonance (NMR) evaluation of Cy-THF solvent system and solution

Cy-THF:DMSO-d_6 (70:30 vol%) solvent mixture was prepared and measured at 300 MHz. ^{1}H-NMR spectrum of fresh and aged solvent brough in ***Figure S3*** provides key insights into the molecular structure, allowing us to assign proton signals to their respective chemical environments. These results confirm the absence of undesirable interactions in both fresh and aged solvent mixtures. Moreover, the proton ratios between Cyrene and 2-MeTHF are in accordance with the given ratio of both solvents for the solution blend.[7,8]

^{1}H-NMR spectra of $MAPbI_3$ for the investigated Cy-THF: DMSO-d_6 (70:30 vol%) solvent system is shown in ***Figure S4***. The presence of $MAPbI_3$ did not cause any unwanted interactions and the solution shows good stability even after aging. The clear signals obtained for the MA^+ ion indicate full dissolution of organic cation. These results support the suitability of Cy-THF for perovskite precursor solutions and are promising indicators of a beneficial implementation in thin film fabrication.

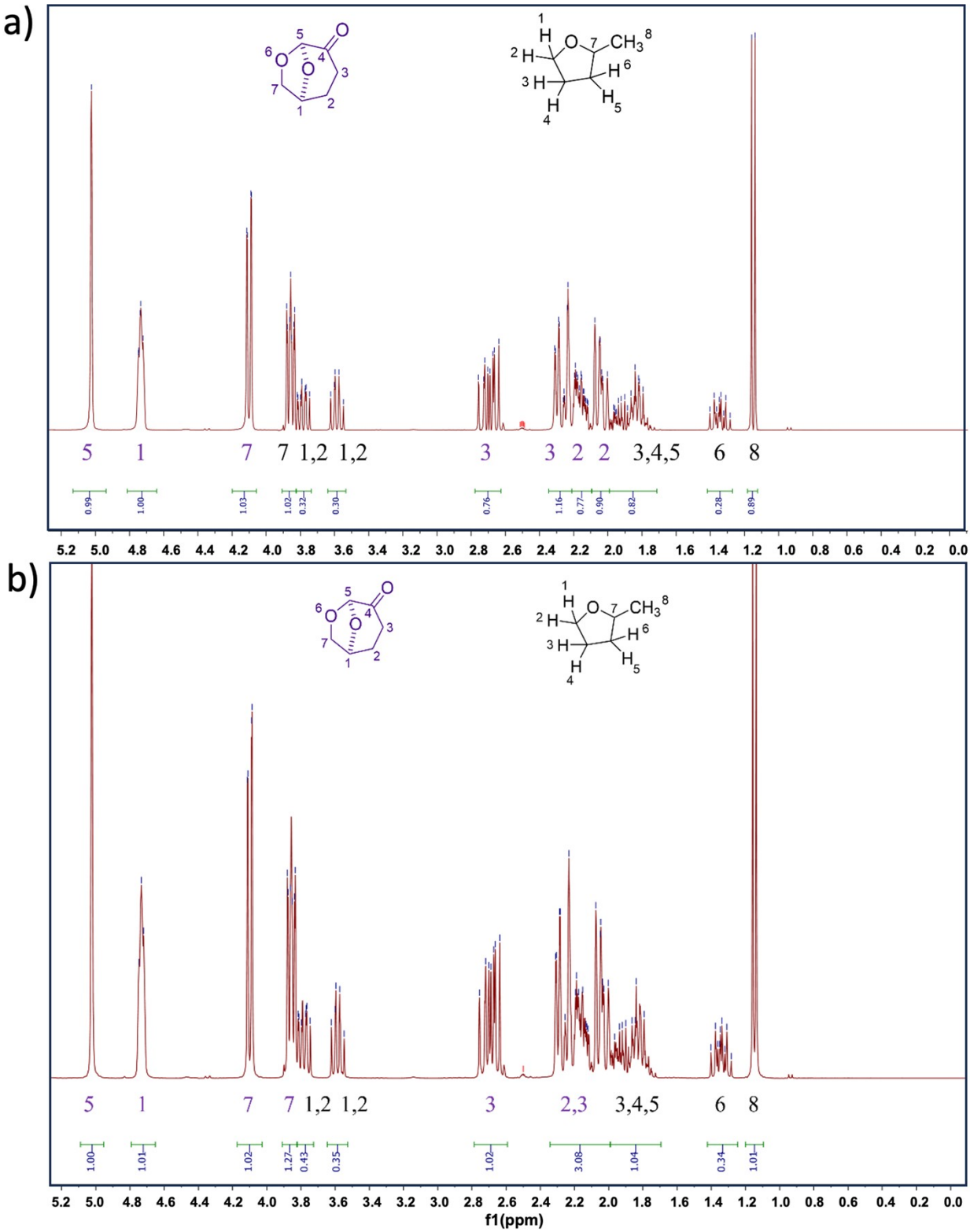

Figure S3: ^{1}H NMR spectrum of Cy-THF:DMSO-d_6 (70:30 vol%) solvent mixture shows the corresponding structures, and the protons assignment to their respective signals. ***(a)*** *Fresh solvent mixture* ***(b)*** *Aged solvent mixture after 7 days. Obtained results match with the known signals for both 2-MeTHF and Cyrene.*

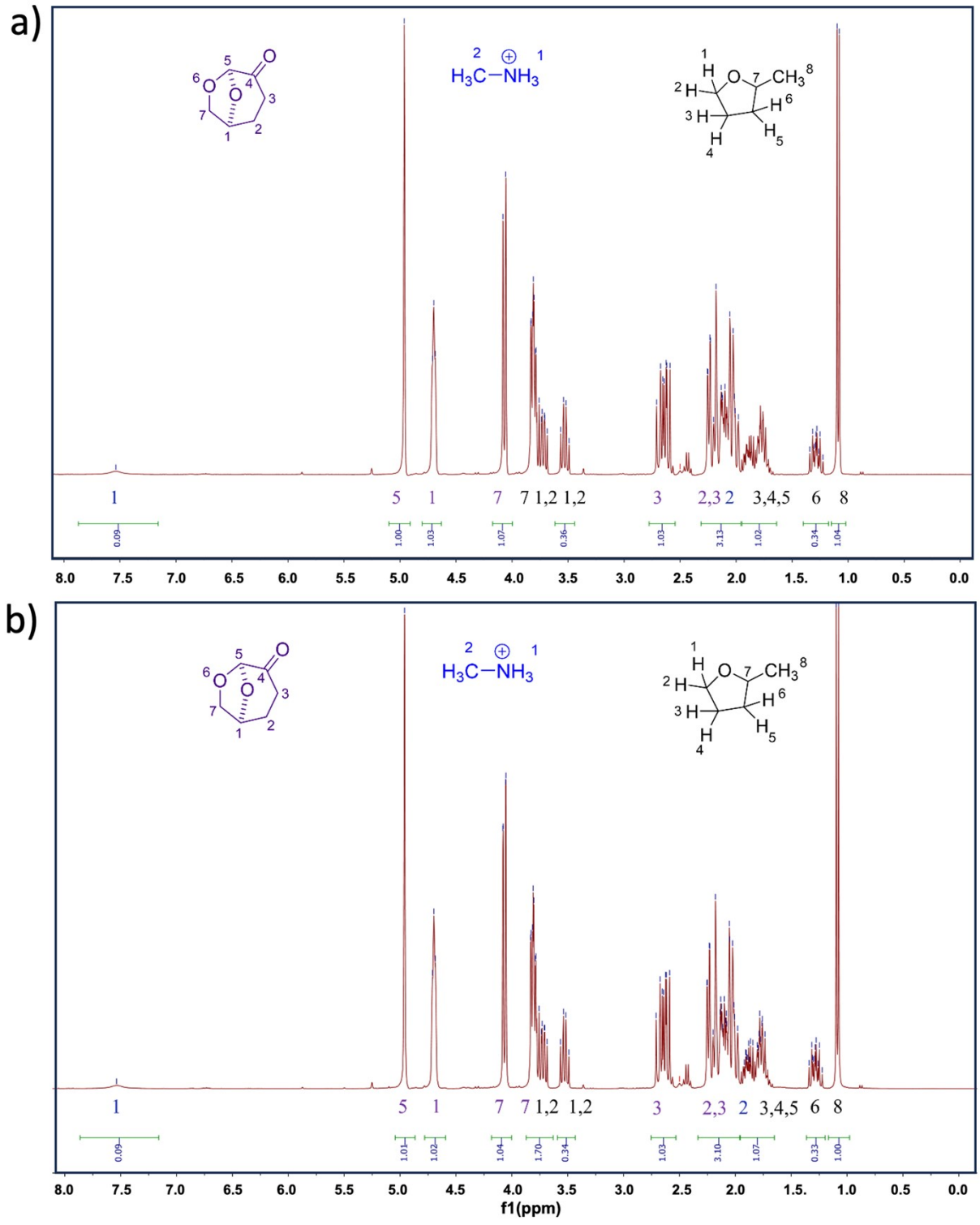

Figure S4: ***(a)*** *^{1}H NMR spectrum of Fresh $MAPbI_3$ perovskite in Cy-THF:DMSO-d_6 (70:30 vol%).* ***(b)*** *Aged $MAPbI_3$ solution after 7 days. The signals for the MA^+ ion are obtained at 7.54 ppm (NH_3^+) and 2.02 ppm (CH_3) respectively.*

2.4 Film coverage and grain size distribution

The films possess a granular morphology, but the grain-to-grain connectivity could be significantly improved and optimized by additives. This improvement is evident in ***Figure S6***, which presents the grain size distribution analysis. The results show a notable increase in average grain size for the green solvent system, exceeding 1.5 µm, more than six times larger than the ~ 225 nm grains observed in the reference DMF:DMSO film. The higher grain growth enhanced film crystallinity but can leave voids that were addressed through chemical additives to obtain nearly pinhole-free films required for better charge transport and overall device performance.

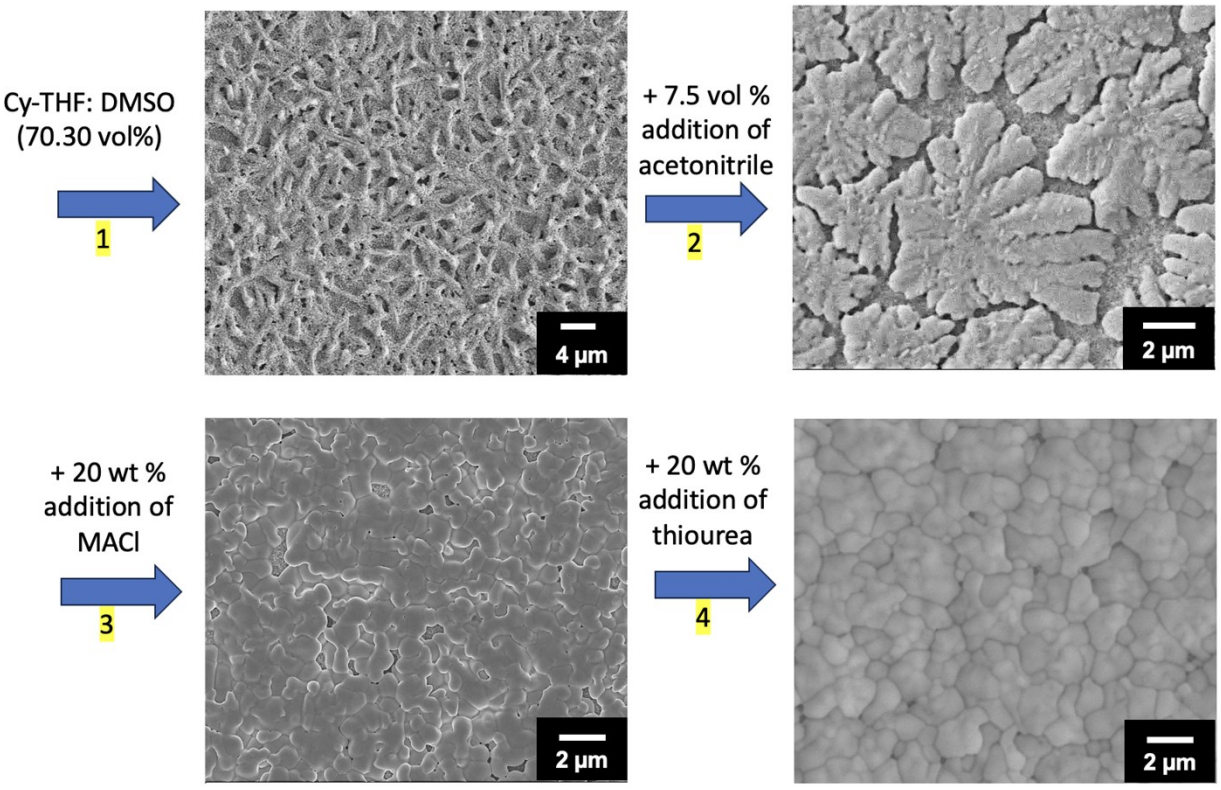

Figure S.5: Stepwise enhancement of surface morphology and film coverage, leading to micron-sized grain formation through additive engineering.

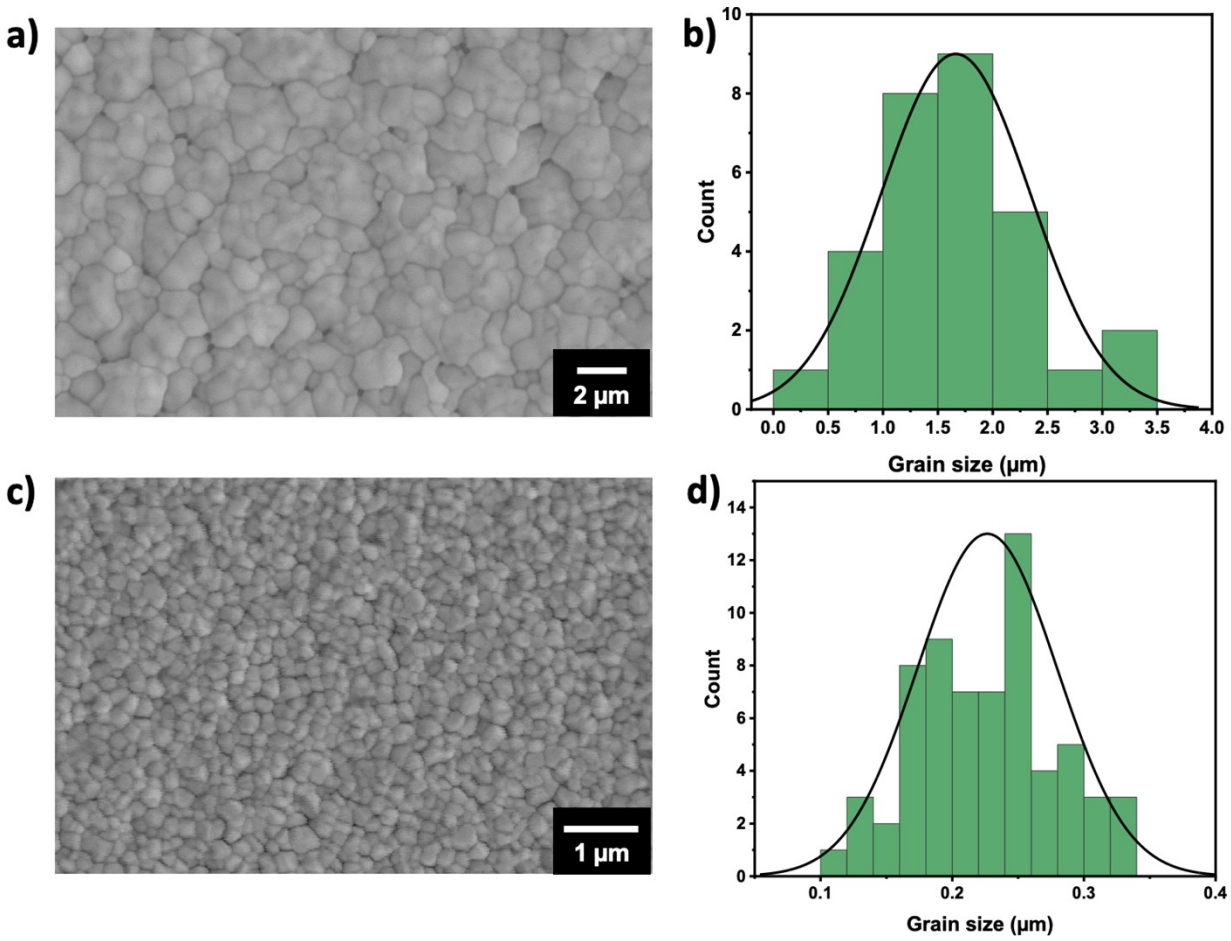

Figure S6: ***(a)*** *SEM image of the film surface processed with the green solvent system.* ***(b)*** *Grain size distribution of the green solvent film, showing an average exceeding 1.5 µm.* ***(c)*** *SEM image of the reference DMF:DMSO-processed film.* ***(d)*** *Grain size distribution of the DMF:DMSO film, exhibiting an average grain size of 225 nm.*

3 References

[1] M. Saliba, T. Matsui, J.-Y. Seo, K. Domanski, J.-P. Correa-Baena, M. K. Nazeeruddin, S. M. Zakeeruddin, W. Tress, A. Abate, A. Hagfeldt, M. Grätzel, *Energy Environ Sci* **2016**, *9*, 1989.

[2] B. J. Kim, H. Choi, S. Park, M. B. Johansson, G. Boschloo, M. Kim, *ACS Sustain Chem Eng* **2024**, *12*, 13371.

[3] X. Cao, L. Hao, Z. Liu, G. Su, X. He, Q. Zeng, J. Wei, *Chemical Engineering Journal* **2022**, *437*, 135458.

[4] K. Schötz, A. M. Askar, W. Peng, D. Seeberger, T. P. Gujar, M. Thelakkat, A. Köhler, S. Huettner, O. M. Bakr, K. Shankar, F. Panzer, *J Mater Chem C Mater* **2020**, *8*, 2289.

[5] J. Sun, F. Li, J. Yuan, W. Ma, *Small Methods* **2021**, *5*.

[6] Y. Miao, M. Ren, Y. Chen, H. Wang, H. Chen, X. Liu, T. Wang, Y. Zhao, *Nat Sustain* **2023**, *6*, 1465.

[7] L. Cseri, S. Kumar, P. Palchuber, G. Szekely, *ACS Sustain Chem Eng* **2023**, *11*, 5696.

[8] N. R. Babij, E. O. McCusker, G. T. Whiteker, B. Canturk, N. Choy, L. C. Creemer, C. V. D. Amicis, N. M. Hewlett, P. L. Johnson, J. A. Knobelsdorf, F. Li, B. A. Lorsbach, B. M. Nugent, S. J. Ryan, M. R. Smith, Q. Yang, *Org Process Res Dev* **2016**, *20*, 661.

[9] M.-R. Ahmadian-Yazdi, A. Rahimzadeh, Z. Chouqi, Y. Miao, M. Eslamian, *AIP Adv* **2018**, *8*.

[10] M. E. O'Kane, J. A. Smith, R. C. Kilbride, E. L. K. Spooner, C. P. Duif, T. E. Catley, A. L. Washington, S. M. King, S. R. Parnell, A. J. Parnell, *Chemistry of Materials* **2022**, *34*, 7232.